ADVANCED FUNCTIONAL MATERIALS

Supporting Information

for *Adv. Funct. Mater.*, DOI: 10.1002/adfm.201904282

Synthesis of Metal Oxide Nanoparticles by Rapid, High-Temperature 3D Microwave Heating

*Geng Zhong, Shaomao Xu, Chaoji Chen, Dylan Jacob Kline, Michael Giroux, Yong Pei, Miaolun Jiao, Dapeng Liu, Ruiyu Mi, Hua Xie, Bao Yang, Chao Wang, Michael R. Zachariah, and Liangbing Hu**

Supporting Information for

Synthesis of Metal Oxide Nanoparticles by Rapid, High-Temperature 3D Microwave Heating

Geng Zhong[1, a], Shaomao Xu[1, a], Chaoji Chen[1, a], Dylan Jacob Kline[2], Michael Giroux[3], Yong Pei[4], Miaolun Jiao[1], Dapeng Liu[1], Ruiyu Mi[1], Hua Xie[1], Bao Yang[4], Chao Wang[3], Michael R. Zachariah[2], Liangbing Hu[1*]

Temperature measurement during microwave heating.

The temperature evolution of the C-wood was estimated by color ratio pyrometry using a Vision Research Phantom Miro M110 high-speed camera, which was used to record the microwave heating video at 2000 frames per second. By taking ratios of the raw channel intensities, most dependent variables associated with the intensity can be eliminated except for those regarding the channel gain (ψ_i), emissivity (ε), and spectral response (χ_i) of the camera at individual wavelengths and channels.[1] For the temperature estimation, we applied the gray-body assumption substituted into Planck's Law, and integrated over the entire spectrum to which the camera is sensitive (as shown in Equation 1 below). The normalized spectral response of the camera for the channel was reported by the manufacturer.[2] When calibrating with a Newport Oriel 67000 Series Blackbody Infrared Light Source, calibration factors C_{gr} (green/red), C_{bg} (blue/green), and C_{br} (blue/red) were determined according to a previous report.[3]

$$\frac{I_i}{I_j} = \frac{\psi_i \int L(\varepsilon, \lambda, T)\chi_i(\lambda)d\lambda}{\psi_j \int L(\varepsilon, \lambda, T)\chi_j(\lambda)d\lambda} \quad \#(1)$$

$$\left(\frac{I_i}{I_j}\right) = C_{ij}\left(\frac{I_i}{I_j}\right)_{\emptyset} \quad \#(2)$$

MATLAB was used to extract raw pixel values and calculate the temperatures of the materials. The demosaicing routine in MATLAB was used with the camera's Bayer color filter array to recover values for the red, green, and blue channels at each pixel. Three color ratios were simultaneously used to estimate temperature by minimizing their summed error with a further thresholding used to eliminate summed errors, corresponding to a temperature error ~110 K. For the temperature profile, only unsaturated pixels above the black level and within the error threshold were used to report the mean and median temperature of the frame for a contiguous area of at least 10 acceptable pixels.

Microwave absorption measurement

The microwave absorption coefficients were obtained from electromagnetic interference (EMI) shielding measurements.[4] When electromagnetic radiation is incident on shielding materials, the coefficient of reflection (R), absorption (A), and transmission (T) must add up to 1, that is $R + A + T = 1$. We obtained R and T from the network analyzer in the form of scattering parameters (S_{mn}), which measure how energy is scattered from a material or device.[5] The first letter "m" designates the network analyzer port receiving the EMI radiation and the second letter "n" represents the port that is transmitting the incident energy. The vector network analyzer directly output four scattering parameters (S_{11}, S_{12}, S_{21}, S_{22}), which can be used to calculate the R and T coefficients as: $R= |S_{11}|^2= |S_{22}|^2$ and $T= |S_{12}|^2= |S_{21}|^2$. Therefore, the absorption coefficient can be calculated as $A= 1- R- T =1-|S_{11}|^2- |S_{12}|^2$.

Thermal conductivity measurement

The thermal conductivities were measured by a steady-state method.[6] The sample was sandwiched between two standard Al blocks with a thermal conductivity of 206 W/m/K. The lower Al block was put on a metal heat sink to introduce heat flux flows through the sample. The

temperature distribution was captured by a FLIR Merlin MID IR camera with a resolution of 320 × 256 pixels.

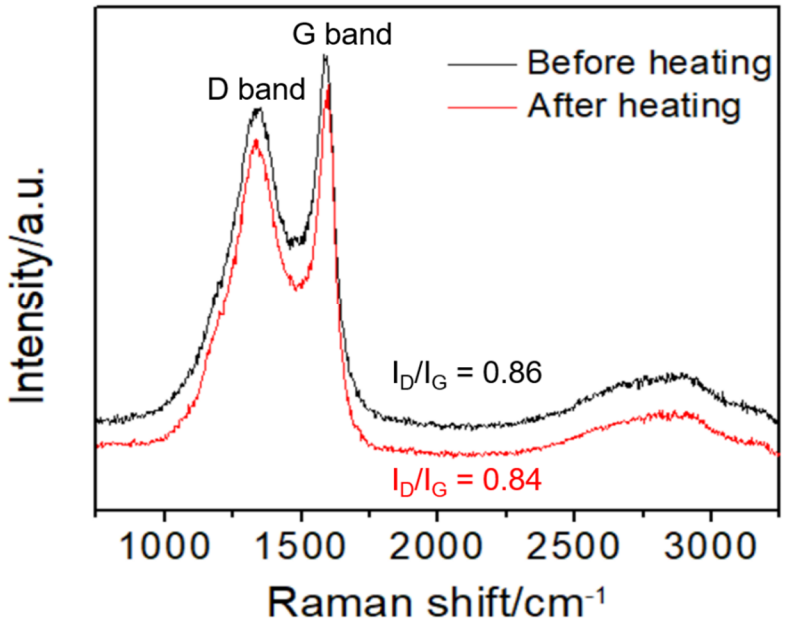

Figure S1. Raman spectra of the C-wood/$Co(NO_3)_2$ before and after microwaving, showing no obvious change after the high temperature 3D heating, suggesting that the rapid heating can effectively avoid damaging or burning the material.

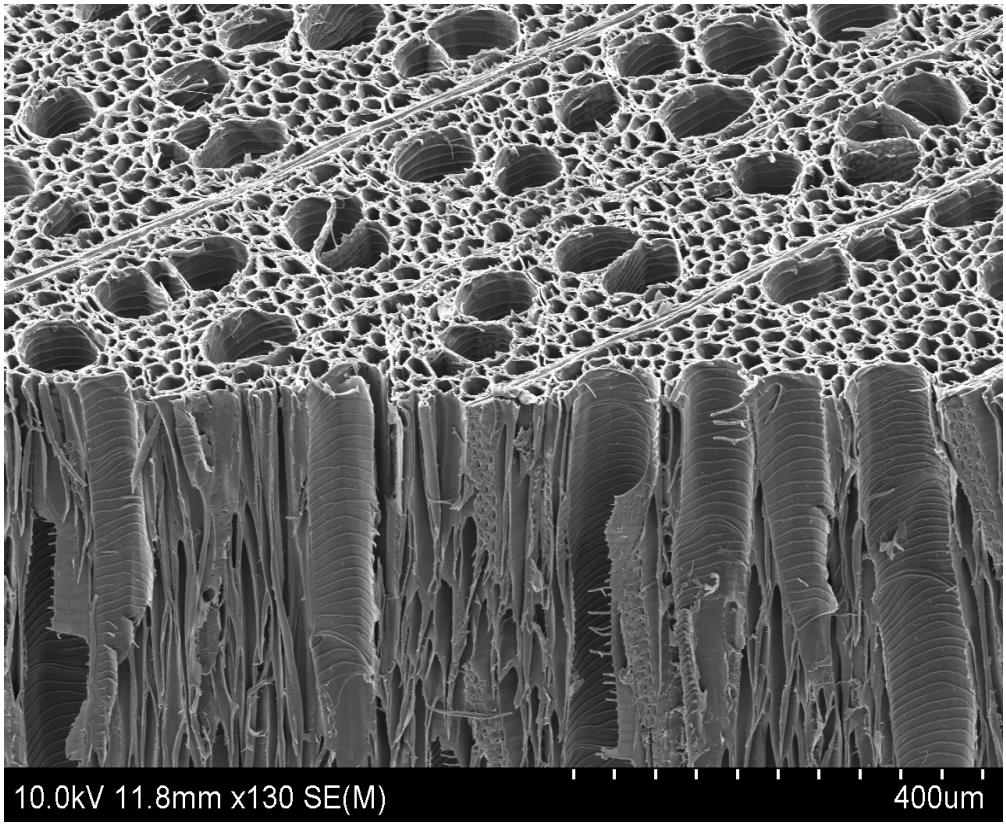

Figure S2. SEM image of the natural wood before carbonization. Hierarchical and regular porous structures with well-defined, aligned channels can be clearly seen in the growth direction. This unique structure is maintained after carbonization.

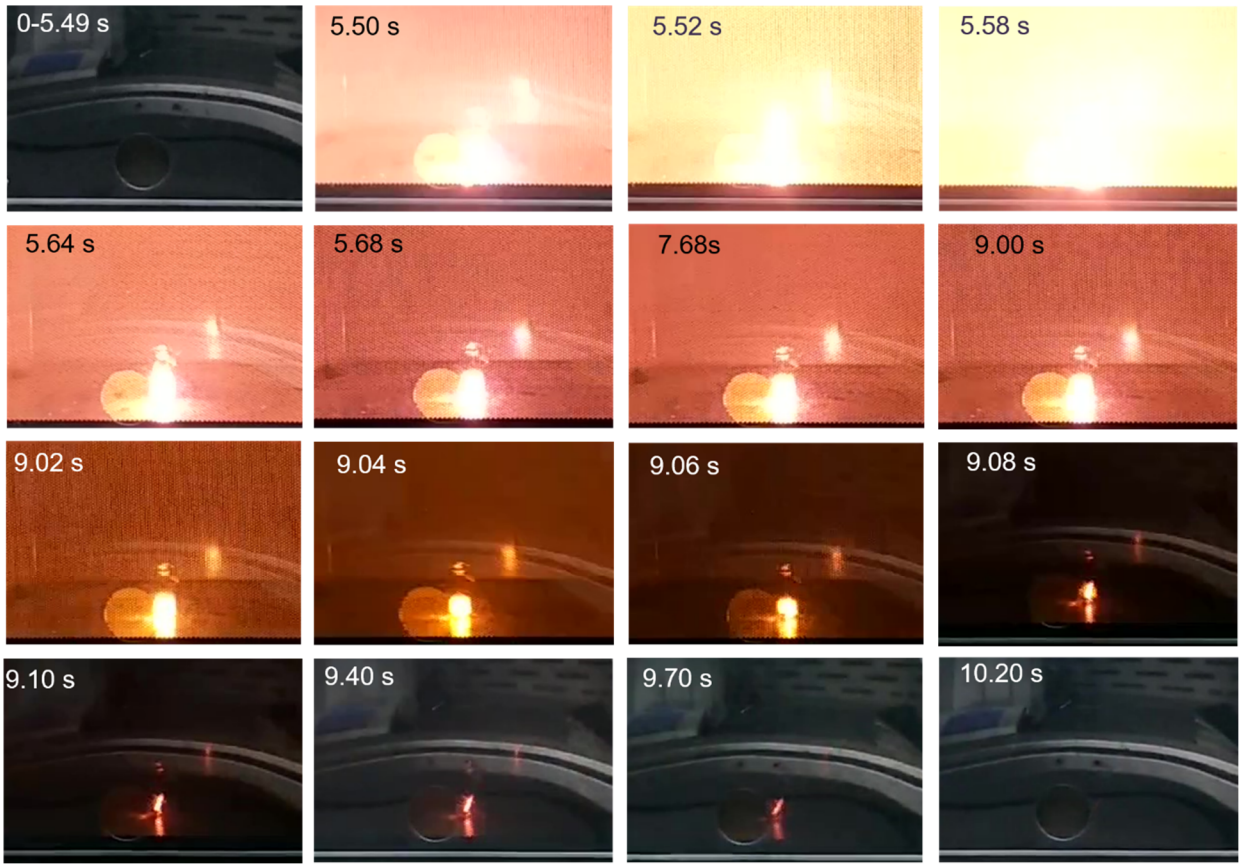

Figure S3. Photos of the of the microwave heating process. This high temperature heating consists of four periods, including induction (~0–5.50 s), rapid heating (~5.51–5.64 s), temperature plateau (~5.64–9.00 s), and cooling (~9.01–10.20 s). The light intensity is consistent with the temperature evolution according to black-body theory.

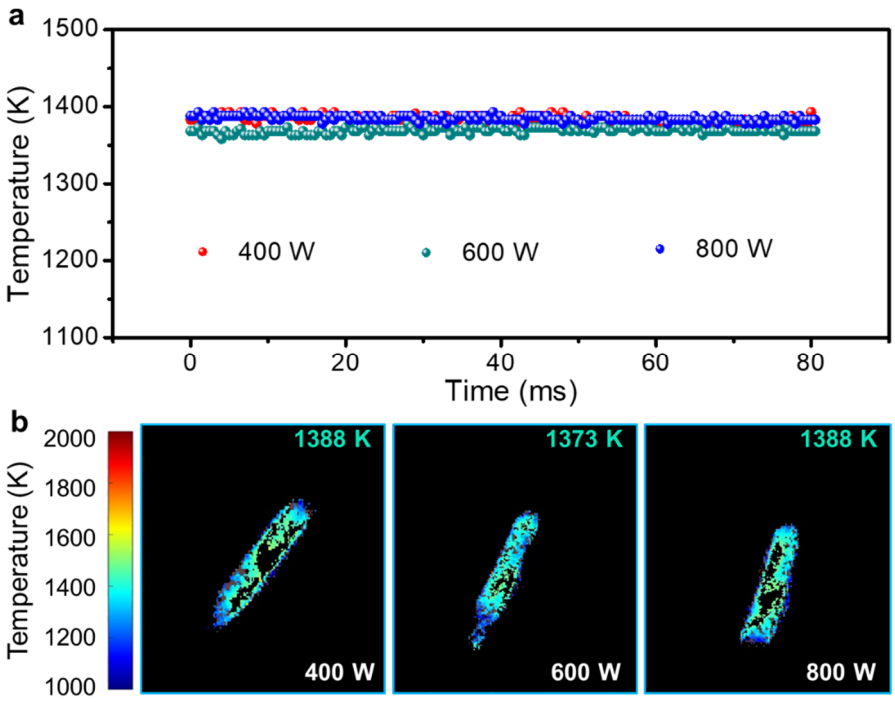

Figure S4. (a) The temporal evolution of temperature estimated from the light intensity according to the black-body theory. (b) The temperature profiles of lighting samples (left, 400 W; middle, 600 W; right, 800 W) calculated from high speed pyrometry frames (captured at 70th ms).

The temperatures of all these three processes are around 1380 K, with the difference less than 30 K (Figure S4a). The corresponding temperature profiles also show similar temperatures (Figure S4b). These results indicate that the microwave power has negligible effect on the temperature of the process. Note that the microwave power affects the preheating time (microwaving time before ignition), which we will further study in another work. It is acceptable that if the microwave power is too low, the limited energy input will not be able to trigger the high-temperature heating.

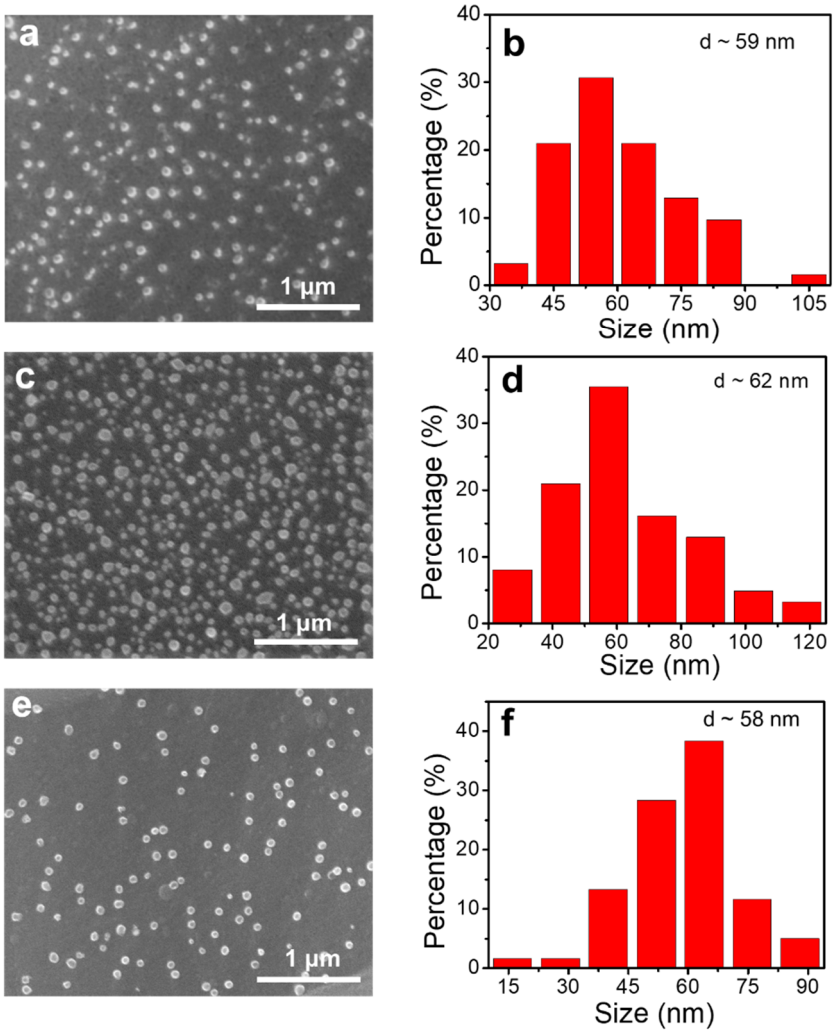

Figure S5. SEM images and size distributions of C-wood/CoO_x synthesized by microwave heating using different microwave powers: (a, b) 800 W, (c, d) 600 W, (e, f) 400 W.

The C-wood supported CoO_x nanoparticles were prepared by 15 s high-temperature heating using different microwave powers (800, 600, 400 W). As shown in Figure S5, the average diameters are ~59, ~62 and ~58 nm, respectively. Such a small diameter difference indicates that the microwave power has negligible effect on the particles size.

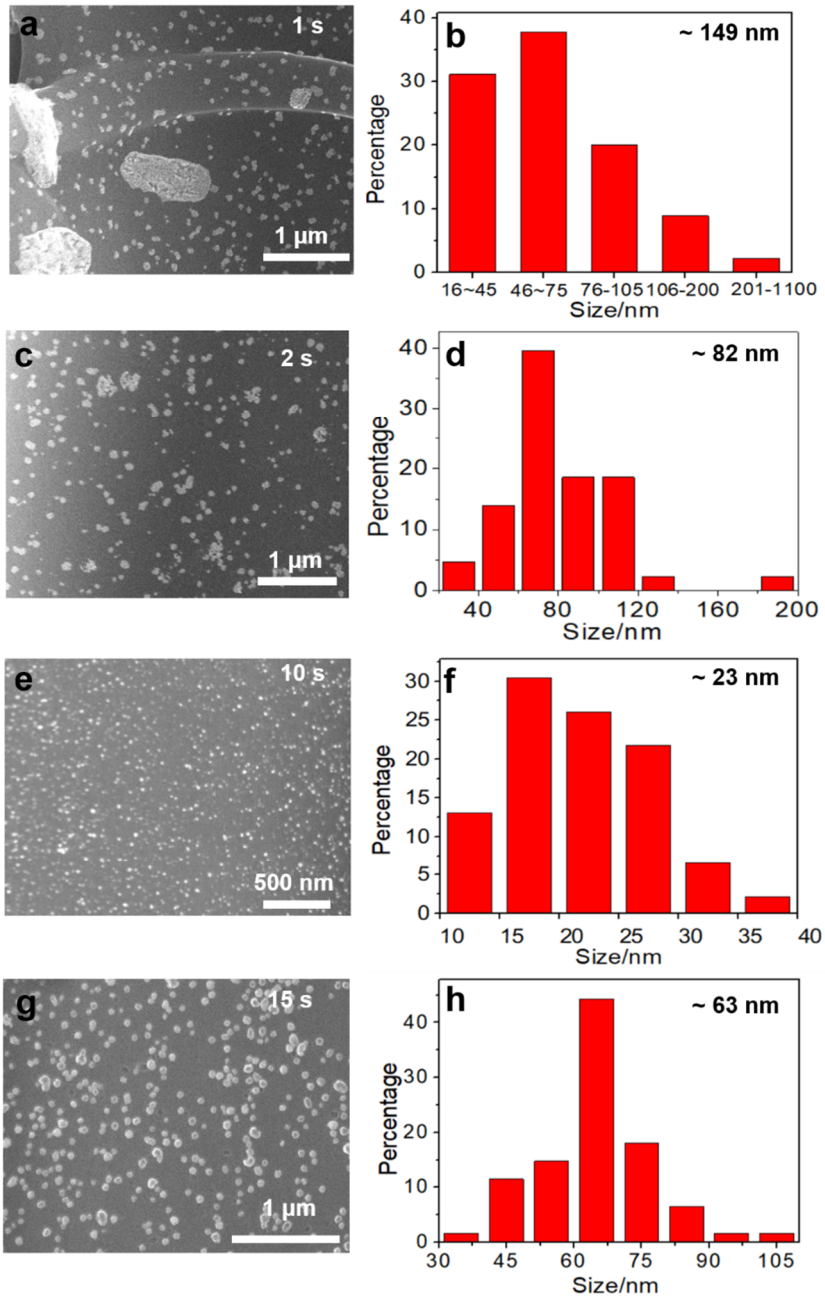

Figure S6. SEM images and size distributions of C-wood/CoO_x synthesized by microwave heating for different times: (a, b) 1 s, (c, d) 2 s, (e, f) 10 s, and (g, h) 15 s.

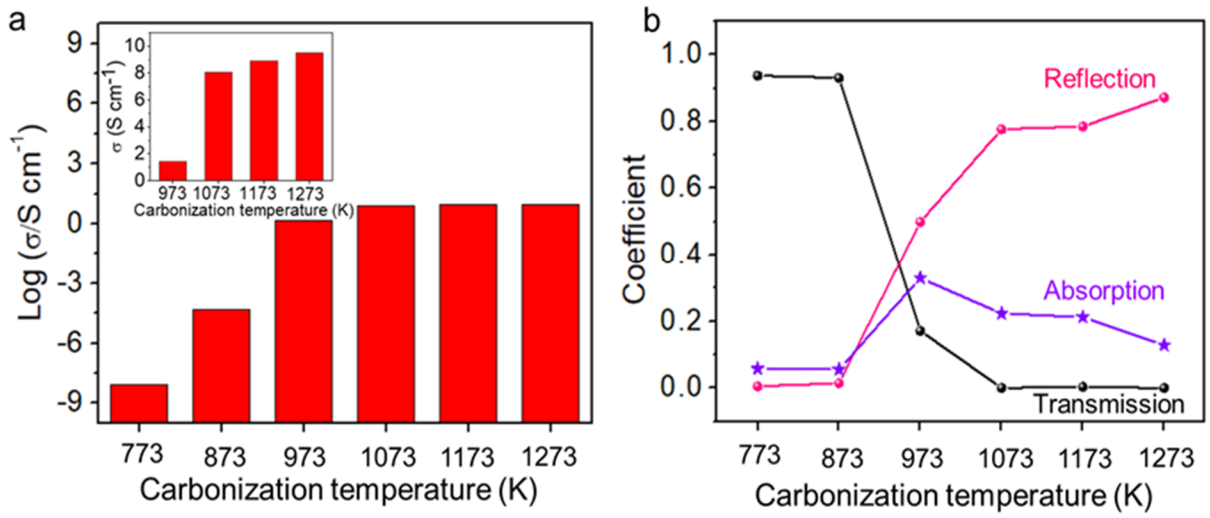

Figure S7. (a) Electronic conductivity (σ) of C-wood made at different carbonization temperatures. (b) The reflection, absorption, and transmission coefficients of C-wood with different σ.

As shown in Figure S7a, the σ increase dramatically by an order of magnitude when the carbonization temperature is below 1073 K and stabilizes to 0 ~ 10 S cm^{-1} above that temperature. Figure S7b shows the reflection, absorption, and transmission coefficients of C-wood with different σ, which can be viewed as the proportion of the incident microwave energy. When the σ is lower than 4.5 $\times 10^{-5}$ S cm^{-1} (C-wood treated at 873 K), the microwaves dissipate mainly by transmission (> 90%). On the other hand, when the σ is higher than 8.1 S cm^{-1} (1073 K treatment), the microwaves dissipate mainly due to reflection (> 78%). Neither of them is effective for triggering the high temperature 3D heating upon microwaving. Only when the σ is close to 1.6 S cm^{-1} can a high temperature be induced.

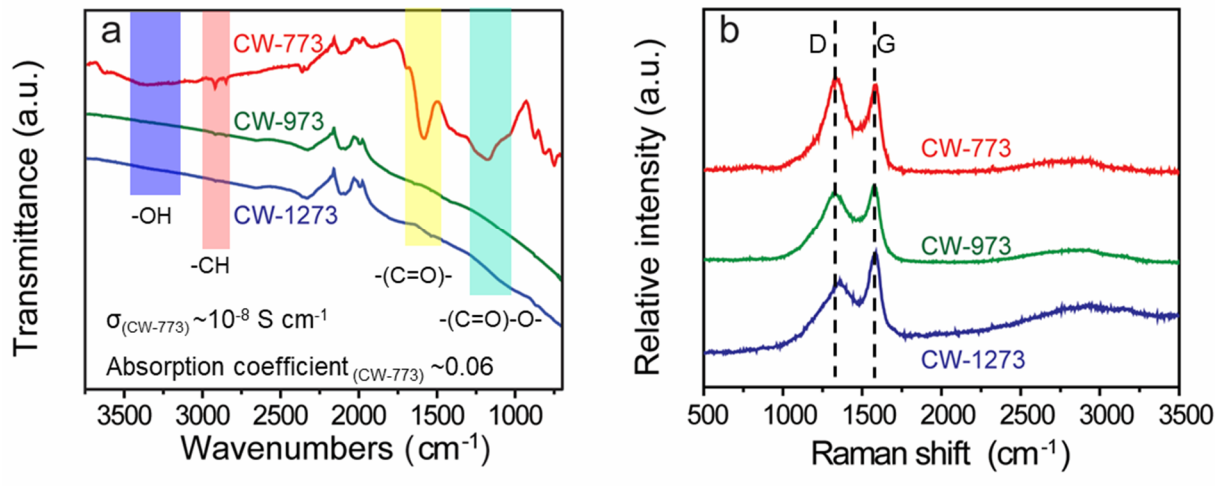

Figure S8. FTIR (a) and Raman (b) of CW-773, CW-973, and CW-1273.

To further study the effect of composition and structure on microwave absorption, we carried out Fourier-transform infrared spectroscopy (FTIR) and Raman spectroscopy to characterize the C-wood carbonized at different temperatures, i.e., 773 K (CW-773), 973 K (CW-973), and 1273 K (CW-1273). The FTIR results show that CW-773 has a higher amount of -OH, -(C=O)- and -(C=O)-O- groups compared with those of CW-973 and CW-1273 (Figure S8a). Meanwhile, the Raman spectrum of CW-500 also shows a higher D-band intensity than that of CW-973 and CW-1273 (Figure S8b), indicating a higher functional group content. The dipoles of these functional groups can rotate in the presence of an electromagnetic field, leading to microwave absorption. However, the microwave absorption coefficient of CW-773 is 0.06, which is much lower than that of CW-973 (0.33) and CW-1273 (0.12) (Figure S7b). Therefore, we conclude that the conductance loss is the primary microwave absorption mechanism in C-wood.

According to the conductance loss mechanism, the oscillating microwave field will lead to a travelling induced current and joule heating within the material. When the carbonization

temperature is low, the high functional group content will lead to a very low electronic conductivity, resulting in the inability to form induced current. In this way, the material can hardly absorb microwave radiation. On the other hand, if the carbonization temperature is high with very low functional group content left in C-wood, the electronic conductivity will be very high that most microwave radiation will be reflected instead of being absorbed (Figure S7b). Only a suitable content of functional group can result in a moderate electronic conductivity, thus leading to a high microwave absorption.

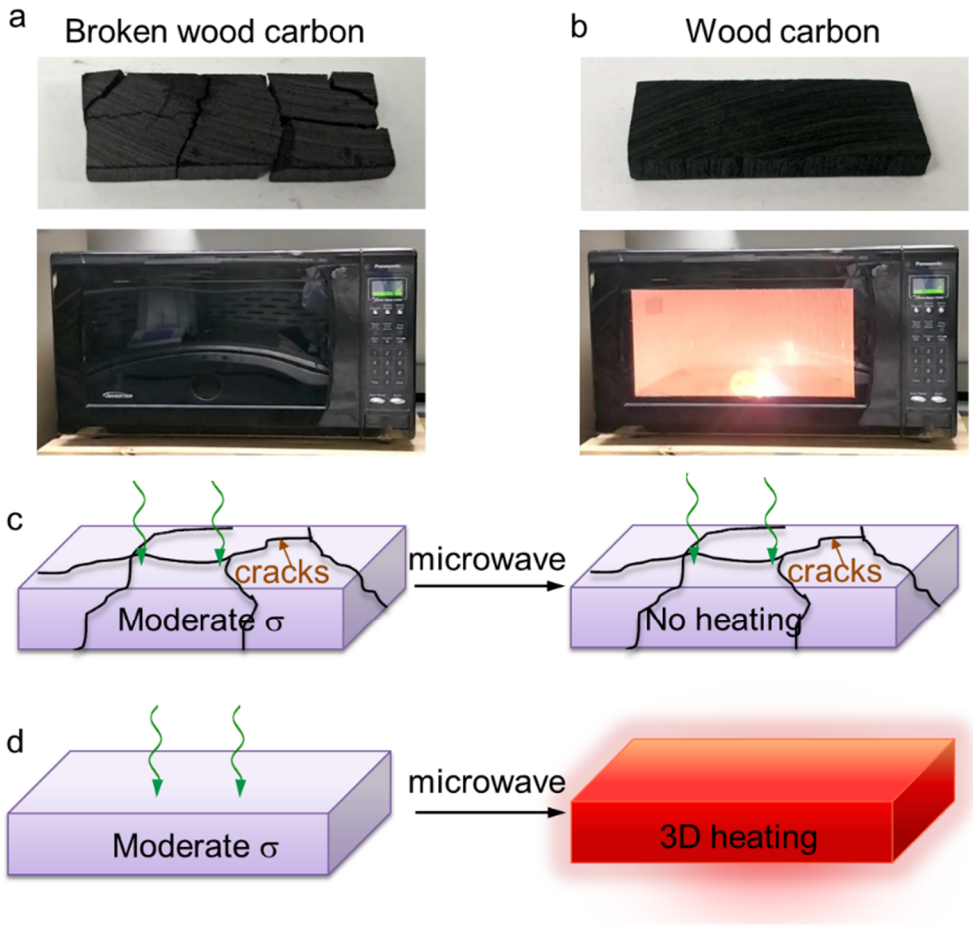

Figure S9. The heating effect of broken C-wood and intact C-wood with moderate electronic conductivity. (a) Photo of the C-wood featuring cracks and its appearance during treatment by 6 s of microwave radiation. (b) Photo of the C-wood without cracks and its appearance during treatment by 6 s of microwave radiation, in which a bright light is clearly emitted, indicating a high temperature has been reached, unlike the cracked sample. (c, d) The corresponding schematics of the cracked and intact carbonized wood upon microwaving.

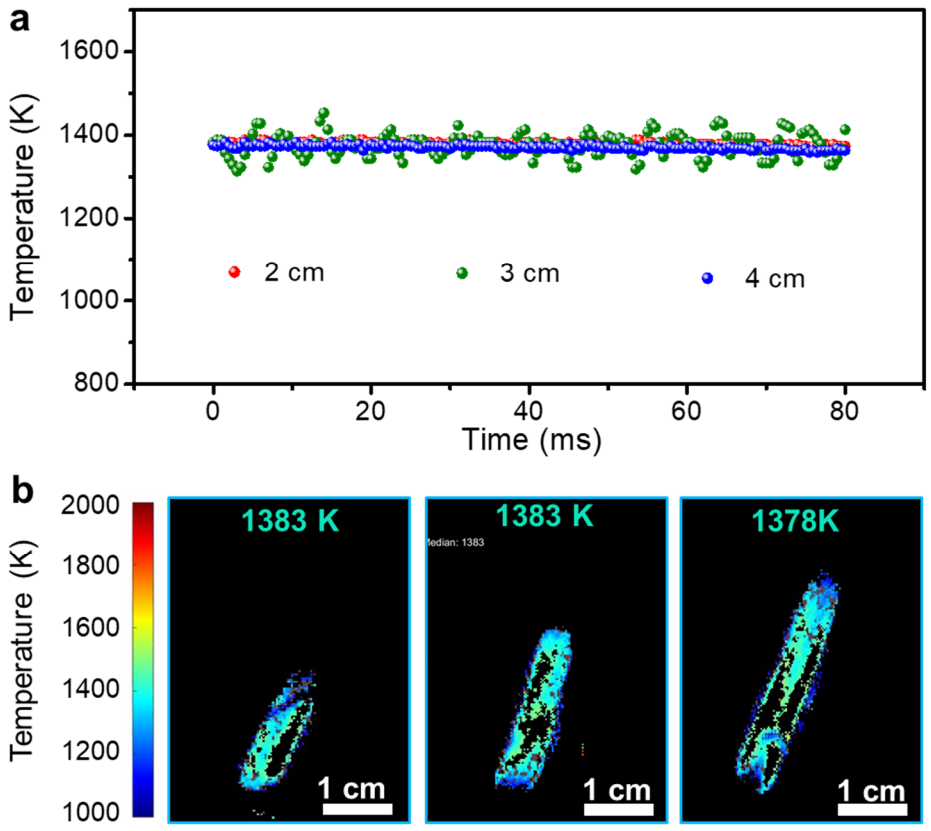

Figure S10. (a) The temporal evolution of temperature estimated from the light intensity according to the black-body theory. (b) The temperature profiles of lighting samples (left, 0.3 cm × 0.4 cm 2.0 cm; middle, 0.3 cm × 0.4 cm × 3.0 cm; right, 0.3 cm × 0.4 cm × 4.0 cm) calculated from high speed pyrometry frames (captured at 70th ms).

References

[1] J. M. Densmore, M. M. Biss, K. L. McNesby, B. E. Homan, *Appl. Opt.*, **2011**, *50*, 2659.

[2] H. Wang, D. Kline, M. Rehwoldt, T. Wu, W. Zhao, X. Wang, M. R. Zachariah, *ACS Appl. Polym. Mater.* **2019**, *1*, 982.

[3] R. J. Jacob, D. Kline, M. R. Zachariah, *J. Appl. Physics* **2018**, *123*, 115902.

[4] D. X. Yan, H. Pang, B. Li, R. Vajtai, L. Xu, P. G. Ren, H. J. Wang, Z. M. Li, *Adv. Funct. Mater.* **2015**, *25*, 559.

[5] J. Ling, W. Zhai, W. Feng, B. Shen, J. Zhang, W. G. Zheng, *ACS Appl. Mater. Interfaces* **2013**, *5*, 2677.

[6] C. Chen, Y. Li, J. Song, Z. Yang, Y. Kuang, E. Hitz, C. Jia, A. Gong, F. Jiang, J. Y. Zhu, B. Yang, J. Xie, L. Hu, *Adv. Mater.* **2017**, *29*, 1701756.